Relative Activity of La_2O_3, LaOCl, and $LaCl_3$ in Reaction with CCl_4 Studied with Infrared Spectroscopy and Density Functional Theory Calculations

Simon G. Podkolzin,† Olga V. Manoilova,‡ and Bert M. Weckhuysen*,‡

The Dow Chemical Company, Core Research and Development, Midland, Michigan 48674, and Departement Anorganische Chemie en Katalyse, Debye Instituut, Universiteit Utrecht, Sorbonnelaan 16, 3584 CA Utrecht, The Netherlands

Received: February 8, 2005; In Final Form: April 11, 2005

Relative activity of La_2O_3, LaOCl, and $LaCl_3$ in the destructive adsorption of CCl_4 to CO_2 was studied with density-functional theory calculations and temperature-programmed reaction experiments monitored with IR spectroscopy. Integral absorbance of the IR peak for phosgene, which is a reaction intermediate, was obtained as a function of temperature, and initial reaction temperatures were compared for different sample amounts of La_2O_3 and LaOCl. The initial reaction temperatures of about 390 K for La_2O_3 and 365 K for LaOCl were practically independent of the tested sample weights, and the lower temperature for LaOCl was attributed to a higher activity of surface sites on this material. Calculations suggest that CCl_4 decomposition proceeds through a stepwise Cl donation from CCl_4 to the surface and that the overall rate is controlled by the first step: CCl_4 splitting into a Cl anion and CCl_3 cation over an acid−base pair of surface sites. A lanthanum acid site in the pair initiates the split by interacting with one of the chlorine atoms in CCl_4, and an oxygen base site stabilizes the remaining CCl_3 fragment. Transition state estimates suggest that the relative activity of surface sites can be ranked in the following order: LaOCl > $LaCl_3$ with a partially dechlorinated surface > La_2O_3. Surface Lewis acidity and basicity of these materials are summarized in terms of the vibrational frequency for adsorbed CO, energy of the lowest unoccupied molecular orbital, and proton affinity. Higher activity of LaOCl is attributed to the higher acidity of the lanthanum site, the higher basicity of the oxygen site, and the geometry of the acid−base pair of sites that allows them to interact with CCl_4 simultaneously.

Introduction

La_2O_3, LaOCl, and $LaCl_3$ materials have been widely studied as active components, promoters, and supports for catalysts in a variety of hydrocarbon reactions. For example, catalysts based on La_2O_3 and LaOCl have been examined for methane coupling,[1−4] for ethane oxidative dehydrogenation,[5,6] and for the conversion of chlorinated methanes into CO and CO_2.[7−9] $LaCl_3$ is used as a component in commercial catalysts in the production of vinyl chloride.[10] Furthermore, LaOCl and $LaCl_3$ have been recently shown to be promising catalysts for selective alkane activation: for methane conversion to methyl chloride,[11] for ethane conversion to vinyl chloride,[12] and for activation of C_{3+} alkanes.[13] In all these reactions, it is important either to limit or, on the contrary, to enhance the conversion of reacting hydrocarbons to CO and CO_2, and therefore, it is desirable to identify the relative catalytic activity of different lanthanum phases.

Our research group focused on the studies of decomposition of chlorinated methanes, such as CCl_4, $CHCl_3$, and CH_2Cl_2 to CO and CO_2 over La_2O_3, LaOCl, and $LaCl_3$ materials.[7−9,14,15] When the decomposition of CCl_4 was conducted catalytically with water vapor, the catalyst composition was found to be dependent on reaction conditions; that is, both the extent of the surface chlorination as well as the bulk composition could change because of diffusion of Cl and O atoms from the surface into the bulk.[9] In a stoichiometric reaction with CCl_4, the apparent reaction rate declined with the transformation of La_2O_3 to LaOCl and then to $LaCl_3$, but the reasons for the decline could not be deconvoluted; it was not clear if the reaction rate was limited by the surface reaction or the bulk diffusion.[7,9] An examination of surface properties of the lanthanum phases with probe molecules allowed us recently to characterize various adsorption sites and showed a general trend in which surface acidity (both Brønsted and Lewis) increases, and conversely, surface basicity decreases in the following order: La_2O_3 > LaOCl > $LaCl_3$.[16]

In this study, we performed temperature-programmed reaction (TPR) measurements monitored with IR spectroscopy for pure La_2O_3 and LaOCl with CCl_4 in order to link the surface properties to intrinsic catalyst activity. We also evaluated the energetics of the considered reactions with electronic-structure calculations based on density functional theory (DFT) and, furthermore, extended these DFT calculations to estimate the reactivity of CCl_4 over $LaCl_3$ with a partially dechlorinated surface, which is a catalyst model of practical significance, but which is difficult to test experimentally because of bulk anion diffusion and thermodynamic instability of the surface. The obtained experimental and theoretical results were used to rank the activity of La_2O_3, LaOCl, and $LaCl_3$ materials, describe their active surface sites, and propose an explanation for the observed differences in the destructive adsorption of CCl_4.

* To whom correspondence should be addressed. E-mail: b.m.weckhuysen@chem.uu.nl.
† The Dow Chemical Company.
‡ Universiteit Utrecht.

10.1021/jp050680y CCC: $30.25
Published on Web 05/19/2005

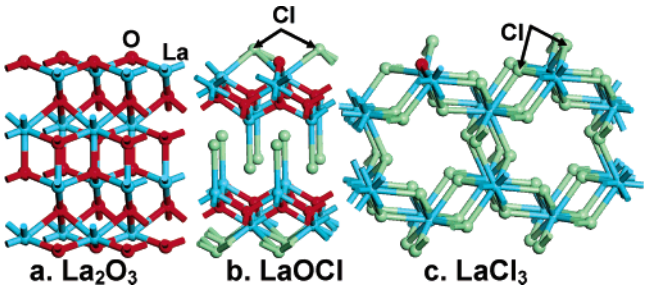

Figure 1. Unit cells of (a) La_2O_3(001), (b) LaOCl(001), and (c) $LaCl_3$(100) used in the construction of infinite periodic models for performing DFT calculations. Arrows indicate chlorine atoms that can be substituted for an oxygen atom to obtain an additional equivalent surface oxygen site on LaOCl and $LaCl_3$.

Experimental Section

1. Materials. A commercial sample of La_2O_3 (Acros Organics, 99.99%) was used without additional purification with the activation procedure described below. A sample of LaOCl was prepared by exposing an equimolar mixture of La_2O_3 and $LaCl_3 \cdot 7H_2O$ (both from Acros Organics, 99.99%) to a 30 mL min^{-1} (g of cat)$^{-1}$ flow of O_2 (Hoekloos, 99.995%) at 1073 K.[4] The purity of LaOCl was confirmed with X-ray diffraction (XRD) and Raman spectroscopy. The XRD measurements were performed using a Siemens D5000 instrument with a 0.154 nm wavelength Ni-filtered Cu Kα source, and Raman spectra were collected with a Holoprobe Kaiser Optical RXN-785 spectrometer.[9] The specific Brunauer−Emmett−Teller (BET) surface area of both samples measured by N_2 adsorption was about 1 $m^2\ g^{-1}$. The density of surface oxygen sites was estimated with CO_2 chemisorption measurements using a Micromeritics 2010 apparatus. Prior to CO_2 titration, samples were pretreated using the same procedures described below. The saturation coverages for chemisorbed CO_2 at 323 K at the final equilibrium pressure of 15 kPa were 0.16 and 0.23 mL g^{-1} (at standard temperature and pressure, STP) for La_2O_3 and LaOCl, respectively. Assuming that the surface area of both samples was exactly 1 $m^2\ g^{-1}$ and that CO_2 forms primarily polydentate species[16] with the stoichiometry of 1 CO_2 for 1 surface O on La_2O_3 and an equimolar mixture of coupled−bridged (2 CO_2 for 1 surface O) and polydentate carbonates (1 CO_2 for 1 surface O) on LaOCl (based on the ratio of IR bands for the two carbonate types[16]), the following surface site density was calculated: 4.3 and 4.7 sites nm^{-2} for La_2O_3 and LaOCl, respectively. For comparison, the densities of oxygen sites for the models in Figure 1 are 7.4 sites nm^{-2} for La_2O_3 and 3.0 sites nm^{-2} for LaOCl terminated with oxygen only. We note that experimental spectra for surface carbonates, theoretical models for different carbonate types, and comparisons between experimental and theoretical vibrational frequencies are described in our previous study on the surface acidity and basicity.[16]

2. Activity Measurements with Temperature-Programmed Reaction Monitored by IR Spectroscopy. For activity measurements, samples were pressed into self-supported wafers (50, 100, and 200 mg) and placed into a stainless steel in situ IR cell equipped with CaF_2 windows. The wafers were positioned away from the IR beam, allowing collection of gas-phase spectra. The La_2O_3 wafers were pretreated in situ in a 400 mL min^{-1} (g of cat)$^{-1}$ flow of 20 mol % O_2 in He (Hoekloos, 99.996%) by raising the temperature to 823 K with a ramp of 10 K min^{-1}, holding at this temperature for 3 h, and then cooling to 323 K in 2 h. The LaOCl wafers were exposed to the same pretreatment but with He only. La_2O_3 forms bulk carbonates by sequestering CO_2 from air. These bulk carbonates decompose at about 1000 K, based on temperature-programmed desorption (TPD) measurements,[16] and therefore, they were still expected to be present after our pretreatment at 823 K. Surface carbonates, however, decompose at a lower temperature of about 650 K,[16] and they were not detected with IR measurements collected with pretreated samples. Carbonates on the surface of LaOCl decompose at about 900 K, according to TPD results,[16] and they were similarly removed in our pretreatment, as was also evidenced by IR measurements. Additional TPD experiments showed that dehydroxylation of the LaOCl surface occurs at about 650 K. Low intensities of OH IR bands, which were similar to those reported earlier,[16] for samples after the pretreatment confirmed that the surface was mostly dehydroxylated prior to activity measurements.

After the pretreatment, samples were exposed to a 40 mL min^{-1} (STP) He flow passed through a saturator with CCl_4 (Merck, 99.8%) at 273 K (effective CCl_4 concentration of 0.047 mol %). The gas flow was controlled with a Bronkhorst mass flow controller. The temperature was raised from 323 to 673 K with a rate of 3 K min^{-1}, and spectral series were recorded by collecting a new spectrum every 2.5 K with a resolution of 4 cm^{-1} using a Perkin-Elmer System 2000 Fourier transform IR (FTIR) spectrometer. The spectral series were analyzed with the *OMNIC 6.0* software.

3. Density-Functional Theory Calculations. Gradient-corrected spin-polarized periodic DFT calculations using the DMol3 code in *Materials Studio 3.0* by Accelrys were performed with La_2O_3(001), LaOCl(001), and $LaCl_3$(100) models reported previously in the study on the surface acidity and basicity of these materials.[16] Briefly, the models were based on a 2 × 2 periodic unit cell with 10 layers for La_2O_3 (40 atoms total), 12 layers for LaOCl, and 16 layers for $LaCl_3$. The bottom layers (7 for La_2O_3, 8 for LaOCl, and 10 for $LaCl_3$) were constrained during the calculations to simulate bulk properties, and the remaining top layers were optimized with an adsorbate. A vacuum spacing of 1.5 nm was used in all surface models. The calculations used the double numerical with polarization (DNP) basis set and the generalized gradient-corrected Perdew−Wang (GGA PW91) functional. Tightly bound core electrons for La were represented with semicore pseudopotentials. Reciprocal-space integration over the Brillouin zone was approximated through *k*-point sampling with a separation of 0.5 nm^{-1} using the Monkhorst−Pack grid: La_2O_3 (3 × 3 × 1), LaOCl (2 × 2 × 1), and $LaCl_3$ (1 × 2 × 1). Convergence with respect to the number of *k*-points was tested by decreasing the *k*-point separation distance to 0.4 nm^{-1} for representative structures. An orbital cutoff distance of 0.5 nm was used for all atoms. All adsorption and surface reaction energies were calculated at 0 K without zero-energy corrections. Transition state searches were performed using a combination of linear synchronous transit (LST) and quadratic synchronous transit (QST) methods with a convergence setting of 0.02 Ha nm^{-1}. The reaction coordinate connecting the reactant, transition state, and product structures (intrinsic reaction path) was estimated with calculations based on the nudged-elastic band (NEB) algorithm with 10 intermediate points.

In agreement with previous experimental and theoretical studies, the (001) plane terminated with oxygen, shown in Figure 1a, was identified as the most energetically stable for La_2O_3.[9] Chlorine-terminated LaOCl(001) and $LaCl_3$(100) were identified as the lowest-energy surface models for the respective materials. Other considered crystal planes and surface terminations were less energetically favorable by 15−80 kJ mol^{-1}. A lattice oxygen site on the surface of LaOCl was generated by substituting two

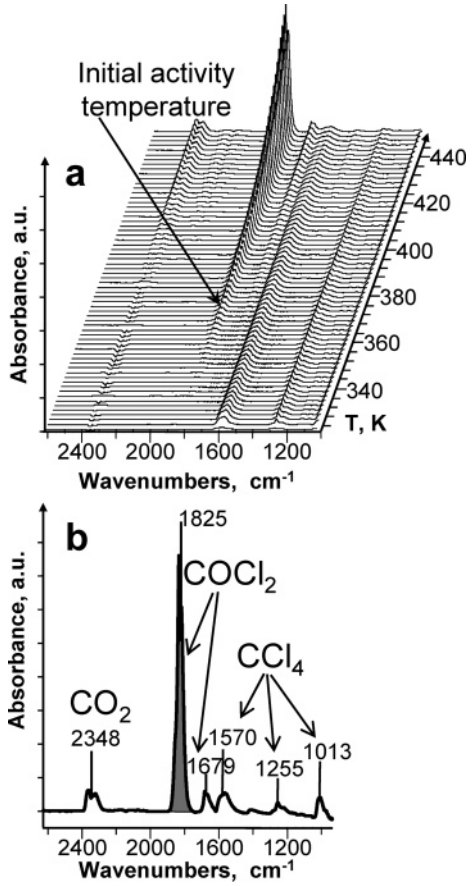

Figure 2. (a) Series of FTIR spectra collected with a 100 mg LaOCl wafer. (b) Spectrum from the series collected at 423 K. The shaded area of the $COCl_2$ peak at 1825 cm^{-1} was calculated to obtain dependences in Figure 3.

terminal Cl atoms in the unit cell. The positions of two remaining terminal Cl atoms, which on substitution for oxygen could generate an additional analogous oxygen site, are marked in Figure 1b. For the $LaCl_3$ model, a substitution of one of the Cl atoms from the top layer and another one from the layer below, as indicated in Figure 1c, was found to be most energetically favorable for generating an oxygen site.

Results

1. Activity Measurements. Previously reported experiments showed that CCl_4 decomposition over La_2O_3 and LaOCl proceeds with the formation of a phosgene ($COCl_2$) intermediate.[7−9] For example, the stoichiometric reactions for LaOCl can be written as

$$LaOCl + CCl_4 \rightarrow LaCl_3 + COCl_2 \quad (1)$$

$$LaOCl + COCl_2 \rightarrow LaCl_3 + CO_2 \quad (2)$$

A representative IR spectral series collected with a 100 mg LaOCl sample with TPR is presented in Figure 2a. The identification of peaks is shown in Figure 2b for the 423 K spectrum from this series. The extinction coefficient for the $COCl_2$ characteristic band is higher than those for CO_2 and CCl_4 in the recorded wavenumber range, and consequently, the $COCl_2$ peak at 1825 cm^{-1} in Figure 2a becomes detectable at 363 K, before the appearance of the CO_2 peak at 2348 cm^{-1} and before any apparent changes in the intensities of the CCl_4 peaks at 1570, 1255, and 1013 cm^{-1}. This sensitivity of the IR measurements to the formation of the reaction intermediate was used

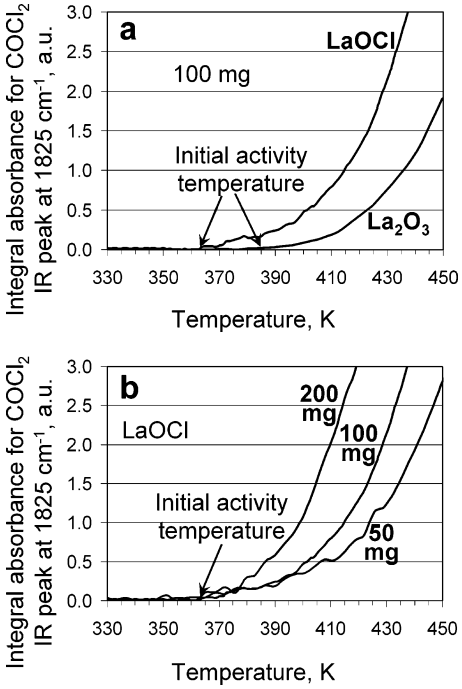

Figure 3. Results of temperature-programmed reaction experiments monitored with FTIR measurements. (a) Comparison of La_2O_3 and LaOCl 100 mg wafers. (b) Comparison of 50, 100, and 200 mg wafers of LaOCl.

for estimating the temperature for the onset of reactivity of CCl_4 with La_2O_3 and LaOCl surfaces. The area for the $COCl_2$ peak at 1825 cm^{-1}, which is shown shaded in Figure 2b, was calculated by integration, and the results are presented as a function of temperature in Figure 3. Since the decomposition of CCl_4 to $COCl_2$ and then to CO_2 represents consecutive reactions (reactions 1 and 2), the concentration of the $COCl_2$ intermediate initially increases with increasing CCl_4 conversion at progressively higher temperatures, as can be seen in Figures 2a and 3.

A comparison of the integral absorbances for 100 mg samples in Figure 3a shows that the initial activity temperature for LaOCl (363 K) is lower than that for La_2O_3 (386 K). The reproducibility of the results in Figure 3a was evaluated with repeat measurements and was found to be within ±3 K. Moreover, the sensitivity of the initial activity temperature to the amount of the solid sample was examined with additional measurements using 50 and 200 mg samples. A comparison of the results collected with different amounts of LaOCl, shown in Figure 3b, indicates that the onset of the reaction is observed at practically the same temperature of about 365 K, regardless of the sample weight. Similar results were obtained with 50, 100, and 200 mg of La_2O_3, and it was found that the initial activity temperature was invariant at about 390 K.

2. Density-Functional Theory Calculations. Previously reported DFT calculations for CCl_4 decomposition over La_2O_3 suggest that the reaction proceeds by a stepwise donation of Cl atoms from CCl_4 to the surface.[9] The first step in this reaction, dissociative adsorption of CCl_4 with the formation of CCl_3 and Cl surface species, was identified as the rate-determining step. In the current study, this initial step of CCl_4 dissociation is evaluated with transition state calculation using the La_2O_3, LaOCl, and $LaCl_3$ surface models shown in Figure 1, and the results are summarized in Figures 4, 5, and 6. These figures provide energy plots as a function of the reaction coordinate (i.e., as a function of the extent of the transformation of gas-phase CCl_4 as a reactant to CCl_3 and Cl surface products). In addition, selected points along the reaction coordinate are

TABLE 1: Acid−Base Properties and Activity of Lanthanum Materials[a]

	La_2O_3	LaOCl	$LaCl_3$
	Lewis Acidity		
ν(CO) experimental, cm^{-1}	2178	2180	2184
ν(CO) calculated, cm^{-1}	2153	2157[b]	2170
		2175[c]	
LUMO energy, kJ mol^{-1}	−177	−208[b]	−297
		−249[c]	
	Lewis Basicity		
ΔE for O^{2-}(surf.) + H^+ = OH^-(surf.), kJ mol^{-1}	−1513	−1595	−1366
	Activity		
E_a for CCl_4 + O^{2-}(surf.) = CCl_3O^-(surf.) + Cl^-(surf.), kJ mol^{-1}	147	nonactivated	109

[a] Calculations were performed with the models in Figure 1. [b] Cl-terminated surface. [c] Mixed O−Cl-terminated surface.

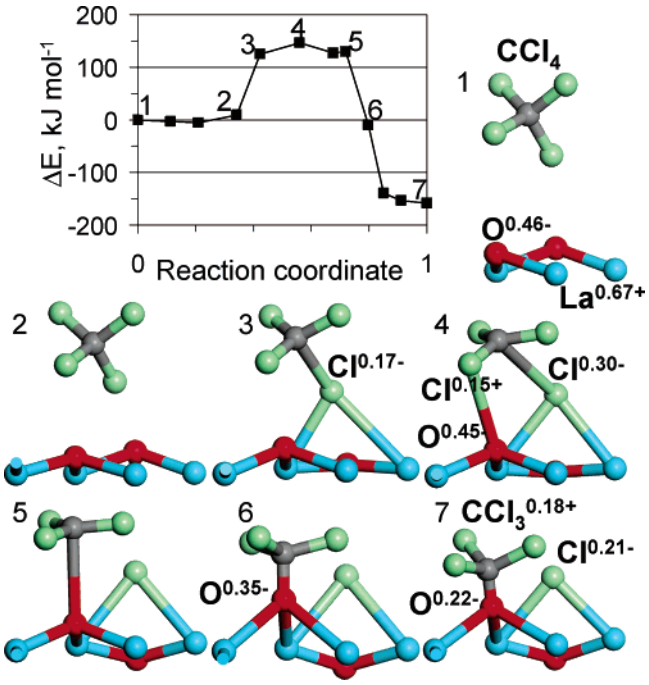

Figure 4. Energy diagram and schematic representation of the reaction pathway for the initial step in CCl_4 decomposition over La_2O_3(001). Only top surface layers are shown for clarity in this figure and Figures 5−7; the full surface models are presented in Figure 1. Numbers next to element symbols in this figure and Figures 5−7 specify partial Hirshfeld charges on atoms and molecular fragments.

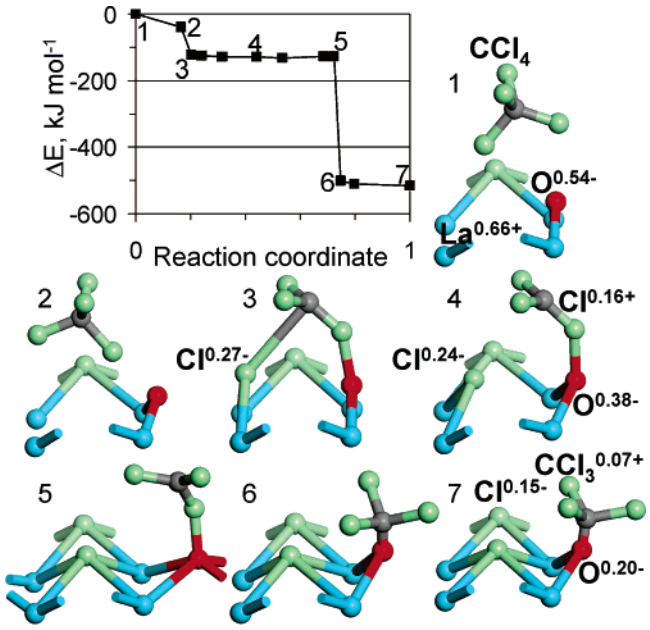

Figure 5. Energy diagram and schematic representation of the reaction pathway for the initial step in CCl_4 decomposition over LaOCl(001).

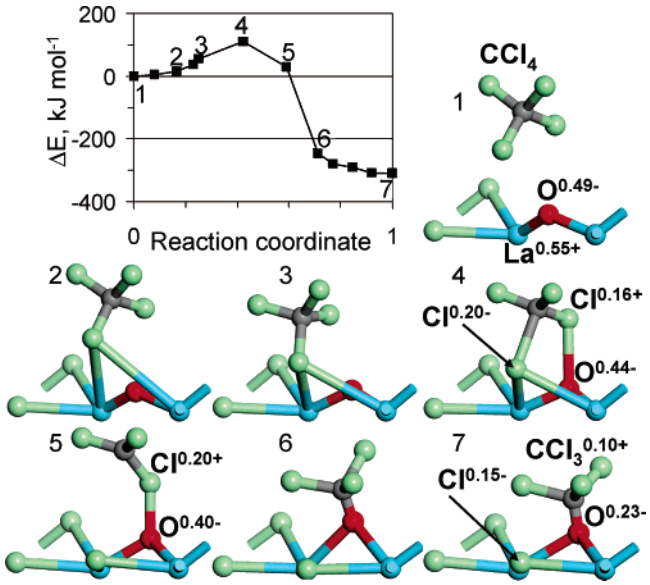

Figure 6. Energy diagram and schematic representation of the reaction pathway for the initial step in CCl_4 decomposition over $LaCl_3$(100).

illustrated with ball-and-stick structures, which show only the top surface layers for clarity. All presented structures are provided as Supporting Information CIF files. The reference in the energy plots is defined as the sum of energies for the corresponding surface model and gas-phase CCl_4 calculated separately or, equivalently, as the energy of a unit cell with CCl_4 being sufficiently separated from the surface so that the interaction between them is negligible. The estimated activation energies are summarized in Table 1. Electron population analysis was performed for all models in Figures 4−7, and essential results are shown in these figures as partial Hirshfeld charges on individual atoms to aid in the description of electronic structure changes.

When gas-phase CCl_4 approaches the surface of La_2O_3 (structure 1 in Figure 4), one of the chlorine atoms in CCl_4 begins interacting with an La Lewis acid surface site. This interaction progressively increases the length of the corresponding C−Cl bond, and this bond becomes progressively more polarized (structure 2 in Figure 4). As the reaction continues, the interacting chlorine becomes an anion and forms a bond with surface La atoms, as shown in structure 3 in Figure 4. The CCl_3 fragment, correspondingly, acquires a positive charge. This charge is mostly localized on the chlorine atom, which is positioned above an O Lewis base site. As the reaction progresses further, this chlorine in the CCl_3 fragment with a partial positive charge becomes stabilized by the surface oxygen site. In the estimated transition state structure in structure 4 in Figure 4, the splitting chlorine anion interacts strongly with the La acid site, while the remaining CCl_3 cation is stabilized over the O base site through its chlorine atom with a positive charge. The CCl_3 fragment then rearranges and bonds to the oxygen site through the carbon atom. As this bond forms, the oxygen site becomes less electronegative, as shown in Figure 4 (structure 6), and the whole structure becomes more stable, as suggested

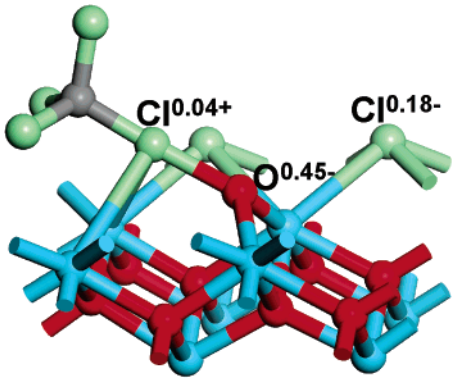

Figure 7. Adsorbed species formed by CCl_4 on the LaOCl(001) surface.

by the energy plot. In the final structure, depicted in Figure 4 (structure 7), the initial CCl_4 is split into two fragments: a $Cl^{\delta-}$ anion bonded to the La acid site and a $CCl_3^{\delta+}$ cation bonded to the O base site, forming the CCl_3-O species. We note that the acid site in this case is an ensemble of three neighboring La cations rather than a single La cation: two of them are shown in structure 7 in Figure 4 as bonding the Cl anion (bond length of 0.29 nm), and another one appears in the projection representation as being below the Cl anion (La−Cl distance of 0.40 nm).

The reaction pathway over LaOCl is similar in terms of the initial interaction and the final structure. Initially, as on La_2O_3, while one of the Cl atoms in CCl_4 begins to react with a La acid site, the remaining CCl_3 fragment is being stabilized over an O base site (Figure 5, structure 2). The interaction with the acid site on the LaOCl surface, however, is stronger, as evidenced by the energetic stabilization of the intermediate structures. In addition, the geometry of the neighboring acid−base LaOCl surface sites allows them to interact simultaneously with two Cl atoms in CCl_4, pulling the molecule apart, as shown in structure 3 of Figure 5. The splitting Cl atom acquires a negative charge and forms bonds with surface La atoms, while another Cl gets a partial positive charge and forms a bond with the O base site early in the reaction. This simultaneous interaction leads to a greater stabilization of the CCl_3 fragment through the formation of a transient $O-Cl-CCl_2$ species, depicted in structures 4 and 5 of Figures 5, and makes the CCl_4 decomposition a practically nonactivated reaction over LaOCl. Similarly to the reaction pathway over La_2O_3, it is energetically favorable for the CCl_3 fragment on the LaOCl surface to rearrange and form a bond with the O site through its C atom (Figure 5, structure 6) rather than to maintain the initial bonding through one of its Cl atoms (Figure 5, structure 5), as indicated by the energy plot in Figure 5. Thus, the final structure in Figure 5 (structure 7) is analogous to the final geometry on La_2O_3 in structure 7 of Figure 4, and it represents the decomposition of CCl_4 with the formation of Cl and $O-CCl_3$ surface species.

Additional calculations for CCl_4 approaching the LaOCl surface suggest the possibility of a stable adsorption state shown in Figure 7. In the identified structure, CCl_4 bonds to a surface O site through one of its Cl atoms, which acquires a small positive partial charge. This Cl atom is additionally stabilized by the neighboring La sites. The calculated adsorption energy is −99 kJ mol^{-1}. In contrast, similar adsorption structures on La_2O_3 and $LaCl_3$ surfaces are significantly less stable with adsorption energies of about 15 kJ mol^{-1}. This difference can be attributed to the greater basicity of LaOCl model O sites, as suggested by the proton affinity results in Table 1.

The reaction pathway over $LaCl_3$, illustrated in Figure 6, is somewhat intermediate: it resembles the transformation over La_2O_3 prior to the transition state and the one over LaOCl after it. Initially, all reaction pathways are analogous (structure 2 in Figures 4−6), because the reaction begins when one of the Cl atoms in CCl_4 starts interacting with an La acid site. The interaction with an La site on $LaCl_3$, however, is relatively strong, and bonds with the interacting Cl in CCl_4 are formed early in the reaction (Figure 6, structure 2). The La site in the case of $LaCl_3$ comprises three La atoms: two of them are shown as bonding in Figure 6 (structure 2), and another one in a lower layer is not shown in this schematic representation. The reaction then progresses similarly to the transformation on La_2O_3, leading to the formation of a $Cl-CCl_2-Cl$ transition state stabilized over a pair of neighboring acid and base surface sites, and the intermediate structures 3 and 4 in Figures 4 and 6 are similar. The calculated activation energy for $LaCl_3$ is 109 kJ mol^{-1}, which is lower than the 147 kJ mol^{-1} estimate for La_2O_3 (Table 1). After the estimated transition state in Figure 6 (structure 4), the reaction on $LaCl_3$ proceeds through the formation of a transient $O-Cl-CCl_2$ species, similarly to the transformation on LaOCl, and structures 5−7 in Figures 5 and 6 are similar. The final geometry in this case, as on La_2O_3 and LaOCl, are Cl and $O-CCl_3$ surface species.

Discussion

Since one of the objectives of the current study is to establish a relationship between surface properties and reactivity, we will briefly summarize here previously reported results on the acidity and basicity of La_2O_3, LaOCl, and $LaCl_3$ surface sites[16] before discussing the activity results. Lewis surface acidity is associated with La^{3+} sites (in this paper, the notation is followed where $\pm n$ refers to a formal oxidation state and $\delta\pm$ to a partial charge on an atom or a molecular fragment). These acid sites can be probed experimentally by, for example, CO adsorption at low temperature. The magnitude of the CO frequency shift on adsorption compared to the gas-phase value of 2143 cm^{-1} can be used as a measure of surface Lewis acidity.[17] The experimental CO frequency values in Table 1, which were collected at low surface coverage, show that surface acidity increases with the extent of chlorination. The calculated CO frequencies in Table 1 confirm this trend. There are two frequencies quoted for LaOCl in Table 1: 2157 cm^{-1} was calculated for a model terminated with Cl atoms only, and 2175 cm^{-1} was calculated for the mixed O−Cl-terminated surface shown in Figure 1b. The difference between these two values suggests that the mixed termination can increase acidity of La sites, as evaluated on the basis of the interaction with CO, and, despite the general trend mentioned in the Introduction, can make the acidity of some sites on the surface of LaOCl actually higher than that of $LaCl_3$ sites (calculated CO frequency of 2175 cm^{-1} for LaOCl is higher than 2170 cm^{-1} for $LaCl_3$). It is inherently difficult to define and rank surface properties with probe molecules, such as CO, because each molecule has not only electronic but also geometric requirements for its adsorption, and furthermore, each molecule inevitably changes the properties of the surface site on adsorption.

This dependence of the probed property on the type of the probe can be avoided by considering computationally only the electronic structure of the surface without any adsorbates or by using a computational probe; for example, a proton that can be expected not to change significantly the surface site. The acidity of the surface, for example, can be estimated by calculating the energy of the lowest unoccupied molecular orbital (LUMO),

which is defined in DFT as the energy change upon addition of an incremental negative charge. The LUMO calculations in Table 1 suggest that surface acidity of the LaOCl model is lower than that of $LaCl_3$ for all considered surface terminations. The apparent difference with the acidity ranking of these models based on CO adsorption, therefore, can be attributed to the geometric site requirements for CO adsorption; that is, the geometry of the model adsorption site on LaOCl allows it to accommodate CO better and, thus, to form a stronger bond despite the fact that its inherent (prior to adsorption) average acidity is actually lower. Basicity of surface sites for La_2O_3, LaOCl, and $LaCl_3$ is difficult to evaluate experimentally, because such probe molecules as CO_2 form different types of carbonates, as evidenced by IR measurements.[16] It is, however, possible to evaluate basicity computationally with proton affinity calculations. The reaction energy for adding a proton to the terminal lattice oxygen site was estimated for the models in Figure 1, and the results are summarized in Table 1. The results for the La_2O_3 and LaOCl models were reported previously,[16] and the value for $LaCl_3$ is reported here for the first time. A comparison of these results suggests that the oxygen site created on the surface of the LaOCl model by the substitution of two Cl atoms is more basic (its proton affinity is higher by 82 kJ mol^{-1}) than the terminal lattice oxygen on La_2O_3. In contrast, the oxygen site on the surface of the $LaCl_3$ model, similarly created by substitution, is significantly less basic than the other two model sites: its proton affinity is lower by 147−229 kJ mol^{-1}.

Experimental observations that the reaction of CCl_4 decomposition into CO_2 can proceed over La_2O_3 and LaOCl without the presence of gas-phase oxygen or water indicate that a surface lattice oxygen can serve as a reaction active site.[7−9] This is consistent with CCl_4 reactions over other metal oxides.[18−21] A further observation that addition of gas-phase oxygen to the reactor feed actually decreases the rate of CCl_4 decomposition over La_2O_3 suggests that adsorbed oxygen does not react with CCl_4 and that surface lattice oxygen is likely to be the primary reaction site.[9] The effect of the gas-phase oxygen addition can be attributed to lower activity of lattice oxygen sites in the presence of adsorbed oxygen species. DFT calculations suggest that CCl_4 decomposition proceeds through a stepwise donation of Cl atoms to the surface,[9] which is consistent with the formation of CCl_x surface species that have been observed spectroscopically on CaO.[20] Initially, one of the C−Cl bonds is activated over a surface acid site, which is associated with lanthanum atoms in the formal +3 oxidation state (La^{3+}); the length of this bond increases, and the activated chlorine atom becomes more electronegative ($Cl^{\delta-}$), while the rest of the molecule becomes more electron deficient ($CCl_3^{\delta+}$). The molecule is then split into a $Cl^{\delta-}$ anion bonded to the La acid site and a $CCl_3^{\delta+}$ cation stabilized by a surface basic site (reaction 3 below). Although the CCl_3 cation has not yet been observed experimentally on La materials, the formation of this fragment was identified as a major reaction pathway in CCl_4 decomposition over small vanadium oxide clusters.[22] On the donation of the second Cl to the surface (reaction 4), a phosgene intermediate is formed, which can desorb (reaction 5) or react further on the surface with another pair of acid−base sites (reactions 6 and 7). The reaction steps can be summarized as follows using formal oxidation numbers:

$$CCl_4 + La^{3+}(\text{surf.}) + O^{2-}(\text{surf.}) \rightarrow La^{3+}Cl^{-}(\text{surf.}) + CCl_3O^{-}(\text{surf.}) \quad (3)$$

$$La^{3+}\ Cl^{-}(\text{surf.}) + CCl_3O^{-}(\text{surf.}) \rightarrow La^{3+}Cl^{-}Cl^{-}(\text{surf.}) + COCl_2(\text{surf.}) \quad (4)$$

$$COCl_2(\text{surf.}) \rightarrow COCl_2 \quad (5)$$

$$COCl_2 + La^{3+}(\text{surf.}) + O^{2-}(\text{surf.}) \rightarrow La^{3+}Cl^{-}(\text{surf.}) + COClO^{-}(\text{surf.}) \quad (6)$$

$$La^{3+}Cl^{-}(\text{surf.}) + COClO^{-}(\text{surf.}) \rightarrow La^{3+}Cl^{-}Cl^{-}(\text{surf.}) + CO_2(\text{surf.}) \quad (7)$$

$$CO_2(\text{surf.}) \rightarrow CO_2 \quad (8)$$

Each combined step of $COCl_2$ formation and $COCl_2$ decomposition to CO_2 corresponds to an exchange of two Cl atoms from CCl_4 for one O atom from the lattice of the solid, and the overall reaction can be written as an exchange of four Cl atoms for two O atoms

$$CCl_4 + 2O^{2-}(\text{surf.}) \rightarrow CO_2 + 4Cl^{-}(\text{surf.}) \quad (9)$$

Chlorine anions can diffuse from the surface into the bulk of the solid, and conversely, oxygen anions can diffuse from the bulk onto the surface.[7−9] This bulk anion diffusion allows a stoichiometric reaction to proceed with a gradual transformation of the solid from La_2O_3 to LaOCl and, finally, to $LaCl_3$. The surface can be dechlorinated by a reaction with, for example, water.[9] The surface dechlorination reaction can be summarized as an opposite of the CCl_4 decomposition: one O atom from water is exchanged for two surface Cl atoms

$$H_2O + 2Cl^{-}(\text{surf.}) \rightarrow O^{2-}(\text{surf.}) + 2HCl \quad (10)$$

Again, because of the bulk anion diffusion, a steam treatment can convert $LaCl_3$ to LaOCl and, finally, to La_2O_3. A catalytic cycle can be constructed by balancing the rates of surface chlorination by CCl_4 and dechlorination by H_2O.[9] The bulk catalyst composition and the extent of surface chlorination, however, can change significantly and equilibrate at dramatically different O to Cl ratios, depending on the initial catalytic material, start-up procedure, and operating conditions. The question then arises if a certain La phase is preferential because of its higher catalytic activity. The catalyst synthesis, pretreatment, and reaction conditions can then be tailored in order to obtain and maintain the preferred state of the catalyst during the reaction. The identification of the preferential catalytic phase is not, obviously, limited to the conversion of CCl_4 into CO_2 but is also important for reactions of other halogenated hydrocarbons, which can be expected to proceed with a similar mechanism. For example, in a reaction of methane oxidative hydrochlorination (reaction 11) over an LaOCl catalyst, formed methyl chloride and other chlorinated methanes can decompose to CO and CO_2, which is an undesirable side reaction.

$$CH_4 + HCl + 0.5O_2 \rightarrow CH_3Cl + H_2O \quad (11)$$

Characterization of the relative activity of lanthanum phases should, thus, provide useful information for all hydrocarbon reactions employing lanthanum catalysts with a variable extent of chlorination.

Catalytic reactivity can be described as being proportional to two factors: the number of active sites and the activity of an

individual site, which is mainly defined by the activation energy

$$\text{reaction rate} \propto \text{site density} \cdot \exp\left(-\frac{E_a}{RT}\right) \qquad (12)$$

The preexponential factor is expected to be primarily defined by the surface collision frequency of gas-phase CCl_4 and, hence, to be similar for different La phases. On the basis of the proposed reaction mechanism, the active site, the density of which is a multiplier in the rate eq 12, is actually a pair of neighboring acid (La^{3+}) and base (O^{2-}) surface sites. The number of oxygen base sites, obviously, decreases with the extent of surface chlorination, and it can be characterized with, for example, CO_2 adsorption, as was done in the current study (the site densities for La_2O_3 and LaOCl were found to be comparable: 4.3 and 4.7 sites nm^{-2}, respectively). In contrast, it is challenging to characterize the intrinsic site activity, because it is difficult to conduct kinetic measurements without affecting both the bulk and surface catalyst compositions. The initial activity measurements with the TPR-IR method reported in this study address this issue. The temperature for the onset of reaction activity depends on the initial reaction rate and the sensitivity of the equipment. Therefore, for a given experimental setup, this initial activity temperature should depend only on the initial reaction rate. Since the reaction rate is only directly proportional to the site density, but in contrast, it depends exponentially on the activation energy (eq 12), the initial activity temperature can be expected to be relatively invariable to the amount of the tested sample and to be sensitive to the activation energy for different sample types.

The results of TPR-IR experiments with 50, 100, and 200 mg samples (LaOCl results are shown in Figure 3b) confirm that the initial activity temperature is practically independent of the sample weight but is consistently lower for LaOCl compared to La_2O_3 samples, as shown in Figure 3a. IR measurements can detect small gas-phase concentrations, and it is estimated that the employed experimental setup allowed us to collect several spectra prior to complete surface chlorination. This is essential for the interpretation of our activity measurements, because once the surface becomes chlorinated, the reaction rate in the employed noncatalytic reaction with CCl_4 becomes determined by the rate of oxygen diffusion from the bulk onto the surface, and the stoichiometry of the surface layers no longer represents the initially tested material. The reproducibility and consistency of the reported initial activity measurements suggest that they are indeed indicative of the surface activity of La_2O_3 and LaOCl prior to the onset of bulk chlorination. The lower initial activity temperature for LaOCl compared to La_2O_3 (365 vs 390 K), thus, suggests that the apparent activation energy for CCl_4 decomposition over LaOCl is lower than that over La_2O_3. Our lower initial activity temperature for LaOCl is also in agreement with reported TPR studies of CCl_2F_2 decomposition analyzed with gravimetric measurements.[23] Although in those studies the experiments were not conducted at identical ramp rates, the fact that the reaction started over LaOCl at a temperature of 180 K lower than that over La_2O_3 suggests higher activity of the LaOCl surface sites. Additional studies suggest that the rate-determining step in the decomposition of chlorofluoromethanes over solid acid catalysts is the first cleavage of a C−Cl bond,[24] and therefore, the initial step in the decomposition of CCl_4 and CCl_2F_2 can be expected to be the same.

Reasons for the higher activity of LaOCl surface sites and the relative activity of $LaCl_3$ were evaluated with DFT calculations. The accuracy of DFT calculations for estimating adsorption energies is usually quoted as being 20 kJ mol^{-1}. This accuracy value depends on the validity of the surface model and computational details. Although our transition state estimates can be expected to be even less accurate than adsorption calculations and, therefore, cannot be used for predicting absolute activation energy values, the presented DFT results should still be useful for predicting activity trends and for rationalizing the predicted relative activity differences. It is currently not clear if decomposition reactions of chlorinated hydrocarbons and specifically those of CCl_4 over La-based catalysts are structure-sensitive, that is, if the reaction rate exhibits a nonlinear dependence on the catalyst surface area. Structure sensitivity would suggest that the reaction proceeds predominantly on defect sites, which become proportionally more abundant for smaller catalyst particles with an overall higher surface area. In the absence of evidence for the significance of defect sites, the reaction was evaluated with simplest models: most energetically favorable crystal planes shown in Figure 1. Furthermore, experiments for the stoichiometric reaction of CCl_4 with La_2O_3 suggest that the presence of surface OH groups is not required for activity.[9] The reaction, accordingly, was modeled only with surface Lewis acid and base sites.

Oxidative hydrochlorination of methane (reaction 11) can be run under conditions when an LaOCl catalyst essentially converts to $LaCl_3$. However, similarly to reactions over La_2O_3 and LaOCl catalysts, it is difficult to vary experimental conditions for kinetic experiments without affecting the bulk composition of $LaCl_3$. Moreover, whereas it is relatively easy to prepare an LaOCl sample with a mixed O- and Cl-terminated surface, attempts to prepare an $LaCl_3$ sample with a partially dechlorinated surface at room temperature usually lead to the formation of dechlorinated subsurface layers due to bulk diffusion, which is evidenced by results of X-ray photoelectron (XPS) and Raman spectroscopic measurements, which were conducted similarly to experiments reported previously.[9] The model of an $LaCl_3$ sample with a partially dechlorinated surface in Figure 1c, therefore, can be viewed as a transient condition of a working catalyst, which is difficult to stabilize under static conditions.

A computational analysis of the CCl_4 decomposition steps on the surface of La_2O_3 (reactions 3, 4, 6, and 7) shows that all these steps are exothermic, and the activation barrier for the elimination of the first Cl is the highest point on the energy diagram.[9] Therefore, the first reaction step of CCl_4 decomposition into CCl_3 and Cl surface species (reaction 3) can be treated as the rate-determining catalytic step under the conditions when the overall rate is not limited by the formation of surface oxygen sites. Consequently, estimates for the activation energy for reaction 3 over La_2O_3 (147 kJ mol^{-1}), LaOCl (nonactivated), and $LaCl_3$ (109 kJ mol^{-1}) model surfaces, reported in Table 1, can be interpreted in terms of relative activity of surface sites of these lanthanum materials. These estimates suggest that the activity decreases in the following order: LaOCl > $LaCl_3$ with a partially dechlorinated surface > La_2O_3. The predicted lower activity of La_2O_3 compared to that of LaOCl is in agreement with the TPR measurements shown in Figure 3a.

The differences in the calculated activation energy estimates can be rationalized by analyzing differences in acidity−basicity and the geometry of active surface sites. The reaction pathways for the initial step in CCl_4 decomposition (reaction 3) in Figures 4, 5, and 6 show that the formation of transition states on all evaluated surfaces involves an activation of a C−Cl bond in CCl_4 over an acid site, which comprises two or three La cations,

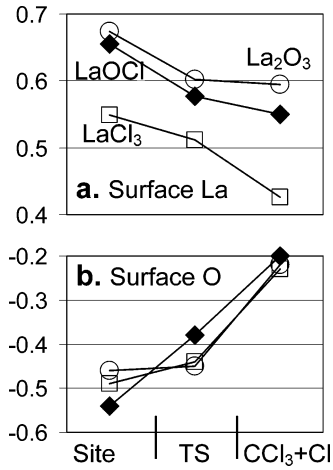

Figure 8. Partial charges on (a) La atom of a surface acid site and (b) O atom of a surface base site for La_2O_3 ○, LaOCl ◆, and $LaCl_3$ □ calculated with the Hirshfeld method. Results are shown for the clean surface sites (Figure 1), transition state structures (structure 4 in Figures 4−6) and initial CCl_4 decomposition products on the surface (structure 7 in Figures 4−6).

bonding of the activated $Cl^{\delta-}$ to this acid site, and simultaneous stabilization of the $CCl_3^{\delta+}$ fragment over a neighboring O base site. This reaction mechanism suggests that higher acidity of the La site should allow it to polarize the C−Cl bond more easily and, similarly, that higher basicity of the O site should allow it to stabilize the $CCl_3^{\delta+}$ fragment more effectively. In addition, the base site should be in proximity to the acid site so that the $CCl_3^{\delta+}$ fragment can be stabilized simultaneously with the abstraction of $Cl^{\delta-}$. A preferable geometric arrangement of the acid−base pair of sites, composing a single active site, should be such that they polarize CCl_4 simultaneously by making one chlorine electron-rich and another one electron-deficient, which can be represented schematically with the following diagram:

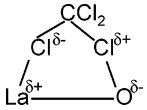

($La^{\delta+}$- -$Cl^{\delta-}$−CCl_2−$Cl^{\delta+}$- -$O^{\delta-}$). The La acid site then abstracts $Cl^{\delta-}$, and the remaining fragment bonds to the oxygen base site, forming transient CCl_2−Cl−O species, which rearrange to a more stable CCl_3−O structure with the bonding through the carbon atom. The extent of participation of La and O surface sites in the reaction can be analyzed by comparing partial charges on the relevant atoms. Some of the computed partial charges are shown in Figures 4, 5, and 6, and in addition, partial charges for an La atom of the acid site and for the base O site for (1) the initial surfaces, (2) the transition states, and (3) the product structures are presented graphically in Figure 8. Since no transition state was identified for LaOCl, partial charges for an intermediate structure in Figure 5 (structure 4) are shown in Figure 8 as a middle point. It is interesting to note that, for clean surfaces, a partial positive charge on La increases in the order $LaCl_3$ < LaOCl < La_2O_3 (Figure 8a), which is the opposite of what is intuitively expected from the acidity ranking. For all surfaces in Figure 8, the partial charge on La decreases, and conversely, the partial charge on O increases in the course of the reaction.

The initial charge on a surface oxygen atom of $LaCl_3$ is lower than that of La_2O_3, as shown in Figure 8b, but it becomes higher in the transition state, indicating a greater participation of the base site in the formation of the transition state on $LaCl_3$. This greater participation occurs despite initially lower basicity of the $LaCl_3$ oxygen site, and it is also manifested by the formation of a transient O−Cl−CCl_2 species after the transition state (structure 5 in Figure 6), whereas such species are not predicted on La_2O_3. This effect can be attributed to a greater polarization of CCl_4 by a more acidic La site on $LaCl_3$, which allows the CCl_2−$Cl^{\delta+}$ fragment to interact more strongly with the $LaCl_3$ base site. A stronger interaction between CCl_4 and the $LaCl_3$ acid site is not directly evident from the changes in the partial charges on La in Figure 8a (the initial slope for $LaCl_3$ is not as steep as that for La_2O_3), because the reacting acid site on La_2O_3 initially comprises two La atoms as opposed to three La atoms on $LaCl_3$. In summary, a lower calculated activation energy for $LaCl_3$ compared to that for La_2O_3 can be attributed to the higher acidity of $LaCl_3$ lanthanum sites, which leads to a greater stabilization of the transition state by the oxygen base site.

The oxygen surface site of LaOCl participates in CCl_4 decomposition even to a greater extent than that of $LaCl_3$, which is evidenced by the steepness of the LaOCl curve in Figure 8b, reflecting changes in the oxygen partial charge in the course of the reaction. This is consistent with the greater basicity of this model site evaluated with proton affinity (Table 1). Intermediate reaction pathway structures 2−4 in Figure 5 suggest that a combination of high basicity of the oxygen site and moderate to high acidity of the lanthanum site (based on CO adsorption and LUMO calculations in Table 1) coupled with the geometry of these surface sites allows them to interact strongly and simultaneously with CCl_4. The higher predicted activity for LaOCl surface sites can, thus, be attributed to this combination of acid−base and geometric effects.

The determined activity ranking of surface sites for CCl_4 decomposition of LaOCl > $LaCl_3$ > La_2O_3 suggests that, in order to increase the reaction rate, CCl_4 decomposition should be run over a dechlorinated surface of LaOCl; a possibly lower number of active surface sites compared to a clean La_2O_3 surface should be compensated by a lower activation energy for the reaction over LaOCl. And, conversely, to minimize complete oxidation in methane oxidative hydrochlorination, the reaction should be run over $LaCl_3$ with as fully as possible chlorinated surface, since this would not only minimize the number of oxidation sites compared to those on LaOCl but would also raise the energetic barrier for oxidation side reactions. The caveat for these recommendations is that they apply only to the discussed conditions where the intrinsic activity of surface sites determines the overall activity. To predict reactivity for a wider range of conditions, the information on the intrinsic activity has to complemented by considering other effects, such as pre-adsorption of reactants (for example, CCl_4 on the surface of LaOCl in Figure 7), formation of lanthanum carbonates by reaction products, presence of surface hydroxyl groups, and, importantly, the rate of formation of surface oxygen sites by either bulk diffusion or by a reaction with an additional reactant, for example, with water.

Conclusions

Temperature-programmed reaction experiments with CCl_4 decomposition to CO_2 over La_2O_3 and LaOCl samples monitored with IR spectroscopy indicate that the reaction starts at a lower temperature over LaOCl. A relative independence of the initial activity temperature of the weight of the tested samples compared to the sensitivity of this temperature to the sample composition suggests that the observed activity difference is primarily determined by the difference in activity of surface

sites rather than in their density. Electronic structure calculations based on density functional theory suggest that CCl_4 decomposition proceeds through a stepwise Cl donation from CCl_4 to the surface. The reaction rate is predicted to be controlled by the first step of CCl_4 splitting into a Cl anion and a CCl_3 cation over an acid−base pair of surface sites. The acid site in the pair, associated with surface lanthanum atoms, initiates the split by interacting with one of chlorine atoms in CCl_4 and by making it $Cl^{\delta-}$, and the base site, associated with a surface oxygen atom, stabilizes the remaining $CCl_3{}^{\delta+}$ fragment. Transition state calculations over model surfaces suggest that the relative activity of surface sites can be ranked in the following order: LaOCl > $LaCl_3$ with a partially dechlorinated surface > La_2O_3. Surface Lewis acidity and basicity of these materials are summarized in terms of the vibrational frequency for adsorbed CO, the energy of the lowest unoccupied molecular orbital, and the proton affinity. Higher activity of LaOCl is attributed to the combined effect of high acidity of La sites, high basicity of O sites, and the geometry of the acid−base site pair that allows CCl_4 to interact strongly and simultaneously with both sites. Intermediate activity of $LaCl_3$ is attributed to higher acidity of La sites but lower basicity of O sites.

Acknowledgment. This work was supported by The Dow Chemical Company. B.M.W. also thanks the Dutch National Science Foundation (NWO-CW) for a VICI grant. We thank the following people at the Dow Chemical Company: E. Stangland, A. Schweizer, R. Maughon, M. Jones, R. Bowman, M. Tirtowidjojo, and P. Margl for useful discussions and M. Olken for help with CO_2 chemisorption measurements. We also thank F. Soulimani and T. Visser (Utrecht University) for help with IR measurements.

Supporting Information Available: Crystallographic information files (CIF) for structures in Figures 1, 4-7. This material is available free of charge via the Internet at http://pubs.acs.org.

References and Notes

(1) Lunsford, J. H. *Angew. Chem., Int. Ed. Engl.* **1995**, *34*, 970.

(2) Campbell, K. D.; Lunsford, J. H. *J. Phys. Chem.* **1988**, *92*, 5792.

(3) Kaddouri, A. H.; De Blasio, N.; Del Rosso, R. *React. Kinet. Catal. Lett.* **2001**, *72*, 309.

(4) Au, C. T.; He, H.; Lai, S. Y.; Ng, C. F. *Appl. Catal., A: Gen.* **1997**, *159*, 133.

(5) Sugiyama, S.; Sogabe, K.; Miyamoto, T.; Hayashi, H.; Moffat, J. B. *Catal. Lett.* **1996**, *42*, 127.

(6) Ciambelli, P.; Lisi, L.; Pirone, R.; Ruoppolo, G.; Russo, G. *Catal. Today* **2000**, *61*, 317.

(7) Van der Avert, P.; Weckhuysen, B. M. *Angew. Chem., Int. Ed.* **2002**, *41*, 4730.

(8) Weckhuysen, B. M.; Rosynek, M. P.; Lunsford, J. H. *Phys. Chem. Chem. Phys.* **1999**, *1*, 3157.

(9) Van der Avert, P.; Podkolzin, S. G.; Manoilova, O.; De Winne, H.; Weckhuysen, B. M. *Chem.—Eur. J.* **2004**, *10*, 1637.

(10) Hodnett, B. K. *Heterogeneous Catalytic Oxidation: Fundamental and Technological Aspects of the Selective and Total Oxidation of Organic Compounds*; Wiley: New York, 2000.

(11) Schweizer, A. E.; Jones, M. E.; Hickman, D. A. U.S. Patent 6,452,058 B1, 2002.

(12) Jones, M. E.; Olken, M. M.; Hickman, D. A. WO Patent 2001038273 A1, 2001.

(13) Schweizer, A. E.; Jones, M. E.; Hickman, D. A. WO Patent 2002094750 A1, 2002.

(14) Weckhuysen, B. M. *Phys. Chem. Chem. Phys.* **2003**, *5*, 4351.

(15) Van der Avert, P.; Weckhuysen, B. M. *Phys. Chem. Chem. Phys.* **2004**, *6*, 5256.

(16) Manoilova, O. V.; Podkolzin, S. G.; Tope, B.; Lercher, J.; Stangland, E. E.; Goupil, J.-M.; Weckhuysen, B. M. *J. Phys. Chem. B* **2004**, *108*, 15770.

(17) Busca, G. *Phys. Chem. Chem. Phys.* **1999**, *1*, 723.

(18) Kiricsi, I.; Nagy, J. B. *Appl. Catal., A: Gen.* **2004**, *271*, 27.

(19) Khaleel, A.; Dellinger, B. *Environ. Sci. Technol.* **2002**, *36*, 1620.

(20) Koper, O. B.; Wovchko, E. A.; Glass, J. A., Jr.; Yates, J. T.; Klabunde, K. J. *Langmuir* **1995**, *11*, 2054.

(21) Ramachandran, B.; Greene, H. L.; Chatterjee, S. *Appl. Catal., B: Environ.* **1996**, *8*, 157.

(22) Bell, R. C.; Zemski, K. A.; Castleman, A. W. J. *J. Phys. Chem. A* **1999**, *103*, 1585.

(23) Bannert, M.; Blumenthal, G.; Sattler, H.; Schoenherr, M.; Wittrich, H. *Z. Anorg. Allg. Chem.* **1978**, *441*, 278.

(24) Tajima, M.; Niwa, M.; Fujii, Y.; Koinuma, Y.; Aizawa, R.; Kushiyama, S.; Kobayashi, S.; Mizuno, K.; Ohuchi, H. *Appl. Catal., B: Environ.* **1996**, *9*, 167.